$^2H(p, pp)n$ reaction at 23 MeV

E. L. Petersen, M. I. Haftel, R. G. Allas, L. A. Beach, and R. O. Bondelid
Naval Research Laboratory, Washington, D. C. 20375

P. A. Treado and J. M. Lambert
Georgetown University, Washington, D. C. 20007,
and Naval Research Laboratory, Washington, D. C. 20375

M. Jain
Texas A&M University, College Station, Texas 77843

J. M. Wallace*
University of Maryland, College Park, Maryland 20742
(Received 12 September 1973)

A kinematically complete experiment that examines the $^2H(p, pp)n$ reaction at several quasifree angles has been performed. The results are compared with calculations performed with a program based on the code of Ebenhöh that solves the Faddeev equations with separable two-body potentials. The calculations are compared with two other programs that use a different integration contour, and the numerical differences are found to be small. The Ebenhöh code is used with three S-wave Yamaguchi potentials. Two of the potentials differ primarily in their predictions of the singlet p-p scattering length. The third potential fits the two-body np and pp scattering data below 30 MeV. The potentials give generally good fits to the breakup data, but do not provide a precise fit to the angular distribution for the quasifree peaks. The potentials themselves differ by about 30% in the predicted quasifree peaks. The calculations explictly show that interference effects are important. It is concluded that a precise fit to the N-N data is not sufficient alone to guarantee a fit to quasifree deuteron breakup data and that the Yamaguchi form factor is inadequate for this purpose.

[NUCLEAR REACTIONS $^2H(p,pp)$, $E=23$ MeV; measured $^3d\sigma$, quasielastic angles. Faddeev calculation, 3 potentials, 3 codes.]

I. INTRODUCTION

An exact theory of the nonrelativistic three-nucleon problem has been available since the work of Faddeev.[1] However, considerable computational difficulties still exist for the N-d scattering problem above breakup threshold for general local (or nonlocal) two-nucleon (N-N) potentials. The theories of Mitra,[2] who pioneered the separable potential approach, and of Amado,[3,4] Lovelace,[5] and Phillips,[6] which employ separable two-body potentials, render the N-d scattering problem tractable. With separable potentials, the Faddeev equations reduce to one-dimensional integral equations that can be solved by standard numerical techniques. Only recently has the more complicated problem of solving the Faddeev equation for simple S-wave local potentials been attempted for breakup.[7]

The initial calculations of deuteron breakup cross sections were compared to single-counter experimental data.[4,8-10] Relatively few kinematically complete experiments have been analyzed with separable potentials.[11-19] Kinematically complete experiments preserve the most information possible since one does not integrate the breakup amplitude over all phase space for one of the particles. Thus, these experiments are useful in the study of certain regions of phase space where results may be sensitive to particular details in the assumed internucleon force.

The inquiry into what nuclear physics can be learned from deuteron breakup experiments requires a great deal of data and many calculations compared with the same data. The data set should be self-consistent as well as consistent with work at other laboratories. Furthermore, the data should be obtained under kinematic conditions such that interesting features are expected. The present experiment is part of a program which is attempting to meet these requirements.

Previous work has shown that there is the greatest difference between (p, pn) and (p, pp) cross sections in the vicinity of 23 MeV[20] and has demonstrated that there is a large difference in the (p, pn) and (p, pp) quasielastic angular distributions.[21] Other laboratories have measured the (p, pp) cross section under similar situations.[22,23] Our previous (p, pp) measurements[21] were obtained under experi-

mental conditions in which it was difficult to observe the final-state interactions. As the results indicated that interference effects were very strong, it was decided to make a detailed study of the reaction at a set of quasifree angles. In this situation, one observes both quasifree scattering (QFS) and final-state interactions (FSI) and does not concentrate on just one or the other. As the relative strengths change drastically, interference effects may show up clearly.

The relative effects of the Coulomb forces are not understood. There is some indication that the exact calculations, excluding Coulomb forces, are adequate to within approximately 1-MeV proton-proton relative energy in the final-state region of phase space.[24] In the present experiment, the p-p relative energies are always above 3.5 MeV, and the p-p angle in its two-body center-of-mass frame is greater than 40°. If Coulomb effects are ever small, it should be under these conditions.

This paper presents the results of a kinematically complete experiment of the $^2H(p, pp)n$ reaction at 23 MeV for several quasielastic angles. The experimental cross sections are compared with those predicted by three separable-potential models. The potentials contain the Yamaguchi form factor,[25] but fit the experimental p-p cross sections over different energy regions. The n-p interactions in the potentials are virtually identical and fit the free n-p cross section up to 30 MeV in the laboratory system (lab).

A separable-potential computer code written by W. Ebenhöh[16] is used to calculate the (p, pp) cross sections. These results are compared with the results obtained from programs written by J. Wallace[19] and by M. Jain,[24] who employ the Cahill-Sloan[10] version of the Amado model.[3] In principle, these programs should give identical results for the same potential. Due to different numerical techniques, however, the three programs give slightly different results, but the computational uncertainty is small compared to the experimental errors. Section III discusses the relative merits of the three programs.

The study of deuteron breakup has reached the stage where one can compare calculations with experiment to see what basic nuclear physics can be learned. This aspect of the problem is discussed in Sec. IV, which compares the results obtained from the different potentials with each other and with experiments. In light of the importance of interference effects[26-28] in determining the cross section, the single scattering, multiple scattering, and their interference contribution to the cross section are calculated. The effects of different contributions to the cross sections, i.e., the p-p and n-p contributions and their interference terms, are also discussed. Section V suggests further calculations and experiments to help elucidate the role of the N-N interaction in explaining the deuteron breakup data.

II. EXPERIMENT

The experiment was performed in a 76-cm Ortec scattering chamber using solid-state detectors. One particle was detected in a ΔE-E telescope with particle identification. The other particle was detected using only an E detector, which facilitated detection of low-energy protons. The fast signals from a timing single-channel analyzer in each leg were taken to a time-to-amplitude converter, which was followed by a stacked single-channel analyzer set for real and accidental times. An "or" between real or accidental events gated the particle identifier. The identification of a proton in coincidence opened gates allowing an E signal, a $\Delta E + E$ signal, and a time signal to go to the analog-to-digital converters (ADC). The E signals could be displayed in a two-dimensional array during a run, and all three signals were recorded on magnetic tape. Later playback with windows set for reals or accidentals produced the final data for analysis. Figure 1 shows a schematic of the electronics.

The target was a CD_2 foil less than 10 μm thick. The use of this target and the bare E detector in

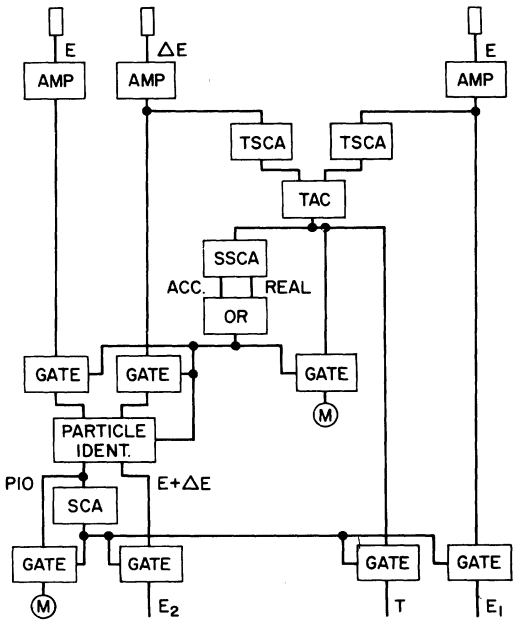

FIG. 1. Block diagram of the electronics used in this experiment. Delays are not indicated. The points designated by M are used during setup and for monitoring of the electronics.

one leg enabled clear detection of low-energy protons. This was checked by observing p-p and p-d elastic scattering at angles such that the scattered proton had a production energy of 1.0 MeV. The detectors had widths of 1° in the horizontal plane and 2° in the vertical plane. The relative coplanar angles of the two detectors were checked by observing p-p elastic scattering in coincidence, and the results indicated that the accuracy was within 0.1°. A fixed monitor at 30° enables the absolute cross section to be obtained from known elastic scattering cross sections. This removes the necessity of accurate measurement of target thickness and integrated beam current.

III. COMPUTATIONAL METHOD

Before presenting the experimental and theoretical results, we compare three computer codes of the Amado[3] (separable-potential) model for the benefit of those who may wish to employ one of these programs in the future. All three codes solve the three-particle Faddeev equations exactly for separable, S-wave, spin-dependent N-N interactions. The N-N potential is of the Yamaguchi form. The programs compared are the following:

Code 1. A code written by Jain and Doolen.[24] This work follows that of Cahill and Sloan[10] with some corrections and modifications appropriate to kinematically complete experiments. For angular momentum $l \leq 3$, the integral equations are solved exactly by matrix inversion with 28-point Gaussian quadrature, with the integration contours of Cahill and Sloan. The second iterative solution of the Faddeev equation is retained for $4 \leq l \leq 5$, while the first iterative solution is retained up to $l = 7$. Born terms are calculated analytically and thus include all partial-wave contributions.

Code 2. A code written by Wallace[19] which again employs the Cahill-Sloan integration contours. The integral equations up to $l = 11$ are solved by iteration to give the Faddeev-Watson multiple scattering series, which is summed by the method of Padé approximates.[7,29] Again, the partial-wave summed Born term is calculated analytically. A 32-point Gaussian quadrature is used for the integrations. The chief difference between Jain's and Wallace's codes is the calculation of the final cross sections from the Faddeev amplitudes. This will be discussed later.

Code 3. A code written by W. Ebenhöh[16] and run by Haftel. Ebenhöh employs integration contours that, unlike the Cahill-Sloan contours, leave the real momentum axis only when necessary. Consequently, the physical "on-shell" amplitude is on the contour of integration. Furthermore, unlike the Cahill-Sloan contours, the contour required in the final-state region [see Fig. 2(b) of Cahill and Sloan and Fig. 2(a) of Ebenhöh] is independent of the final-state momentum. The solution of the integral equations is obtained by matrix inversion for $l \leq 2$, by first iteration for $3 \leq l \leq 5$, and from the Born term for $l \geq 6$. The contours are divided into three regions, each of which is integrated over by a Gaussian quadrature formula, with a combined total of 31 points.

Each code has its advantages. Code 1 has been very carefully checked and probably has the least computational inaccuracy. Code 2 provides the multiple scattering series as a by-product of the Padé approximant method. Codes 1 and 3 are very

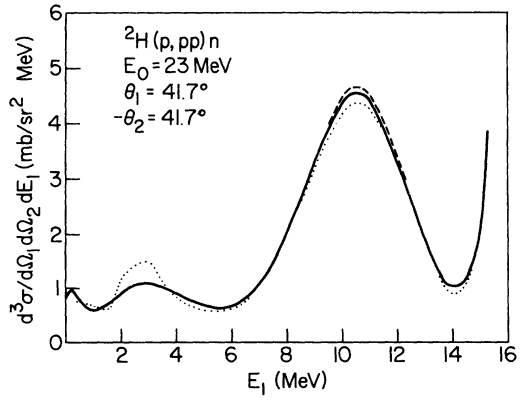

FIG. 2. The results produced by three different "exact" codes for calculating deuteron breakup cross sections. — code of Ebenhöh, --- code of Jain and Doolen, ••• code of Wallace. The angle pairs are on opposite sides of the plane for all of the cases in this paper.

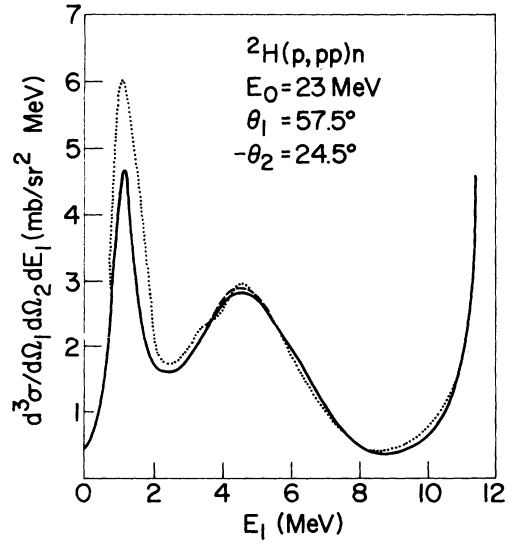

FIG. 3. The results of three different calculations of deuteron breakup. Curves correspond to those of Fig. 2.

compact and useful for experimentalists. Figures 2 and 3 illustrate the $^2H(p, pp)n$ cross sections as calculated by the three codes at two pairs of quasielastic angles. All calculations are for the "Y-Y model" of Cahill and Sloan,[10] which corresponds to the potential A of Sec. IV of this paper. The codes give almost identical results with a maximum spread of about 7% at the quasifree scattering peak at $\theta_1 = -\theta_2 = 41.7°$. As one proceeds closer to the FSI region, the Ebenhöh and Jain results become very close, but the Wallace results are in some disagreement.

Near the QFS peak one needs only amplitudes calculated on the "simple" contours [Fig. 2(a) of Cahill and Sloan and Fig. 2(b) of Ebenhöh]. Both of these contours stay sufficiently far from singularities in the three-body propagator so as to present no serious numerical difficulties.

As one proceeds away from the QFS peak, amplitudes calculated on the more "complicated" contours [Fig. 2(b) of Cahill and Sloan and Fig. 2(a) of Ebenhöh] come into play. In this region there is a Born-term propagator singularity on the second sheet at zero momentum. This singularity is removed by a phase-space factor in the integral equation, but it does lead to a peaked kernel near zero momentum; therefore, one has to be careful handling this integral numerically, since large cancellations occur in the integration on the second sheet. The fact that Ebenhöh and Jain get nearly the same result encourages one to believe the numerical evaluations were handled adequately. Furthermore, the Ebenhöh and Jain "complicated" contour amplitudes are numerically stable—e.g., their amplitudes usually do not change more than 1% as one doubles the number of integration points. On the other hand, Wallace's amplitudes possess small discontinuities which apparently arise from the integration technique employed. One of the encouraging points of Ebenhöh's contour is that he gets a numerically stable result with fewer integration points [16 points on segment 0-1-2-3-4 of his Fig. 2(a) versus 40 points in the Jain code for segment AB of Fig. 2(b) of Cahill and Sloan].

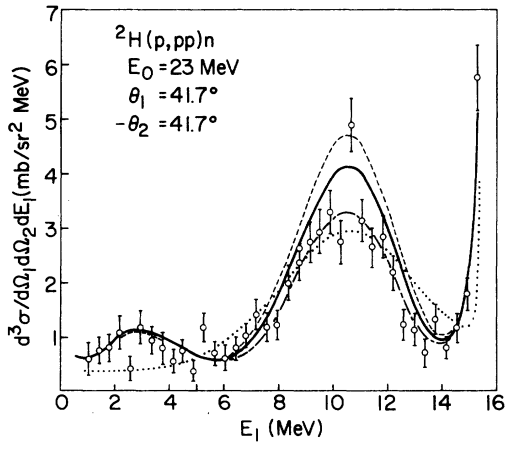

FIG. 4. Observed and calculated spectra. Three of the curves were obtained using the three different nucleon-nucleon potentials: A (--), B (— -), and C (——), discussed in the article. The fourth curve (• • •) represents the Born terms for potential B ($\times \frac{1}{5}$).

Differences in predictions of the three codes can come from two sources: (1) different calculated Faddeev amplitudes, and (2) details in calculating the cross section from the amplitudes. Table I compares the amplitudes calculated from the three codes for selected values of the final momentum (q_i), angular momentum (l), total spin (S), and two-body substate [singlet ($s_i = 0$) or triplet ($s_i = 1$)]. The amplitudes correspond to the quantity $T_{i,I}(q\sigma)$ of Eq. (17) of Ebenhöh, where the final state (σ_i) has spin quantum numbers S, s_i; and the initial state (σ) has quantum numbers $S, s = 1$. The quantity q is the on-shell initial momentum $q = (E + \kappa_0^2)^{1/2}$ where E is total center-of-mass energy and κ_0^2 is the deuteron binding energy.[30] The disagreement is usually less than 1%, except for Wallace's amplitudes for large q_i. The agreement between the

TABLE I. Faddeev amplitudes for Y-Y model (potential A) as calculated by three computer codes.

q_i (MeV$^{1/2}$)	l	S	s_i		$T_{il}(q\sigma)$ ([MeV]$^{-5/4}$) (1) Jain $\times 10^{-3}$	(2) Wallace $\times 10^{-3}$	(3) Ebenhöh $\times 10^{-3}$
3.062	0	$\frac{3}{2}$	1	Re	−4.1809	−4.1580	−4.1737
				Im	−5.7297	−5.7255	−5.7164
	1	$\frac{3}{2}$	1		−0.5322	−0.5342	−0.5316
					0.4920	0.4890	0.4895
	2	$\frac{3}{2}$	1		0.4319	0.4289	0.4310
					−0.8513	−0.8463	−0.8489
	0	$\frac{1}{2}$	0		−0.7786	−0.7796	−0.7744
					0.2859	0.2822	0.2861
	1	$\frac{1}{2}$	0		2.3106	2.3107	2.3062
					2.4427	−2.4259	2.4358
	2	$\frac{1}{2}$	0		−0.4482	−0.4438	−0.4464
					−0.6336	−0.6307	−0.6315
3.547	0	$\frac{3}{2}$	1		−5.4694		−5.5098
					−7.2713		−7.2905
	1	$\frac{3}{2}$	1		−1.8394	−1.7670	−1.8341
					−1.1072	−0.9740	−1.1095
	2	$\frac{3}{2}$	1		0.7270	0.7297	0.7252
					−0.9815	−0.9616	−0.9816
	0	$\frac{1}{2}$	0		1.2745		1.2643
					2.7314		2.7614
	1	$\frac{1}{2}$	0		6.1921	5.7372	6.0962
					1.2514	1.4975	1.2786
	2	$\frac{1}{2}$	0		0.2800	0.2310	0.2618
					−1.6489	−1.4830	−1.6373

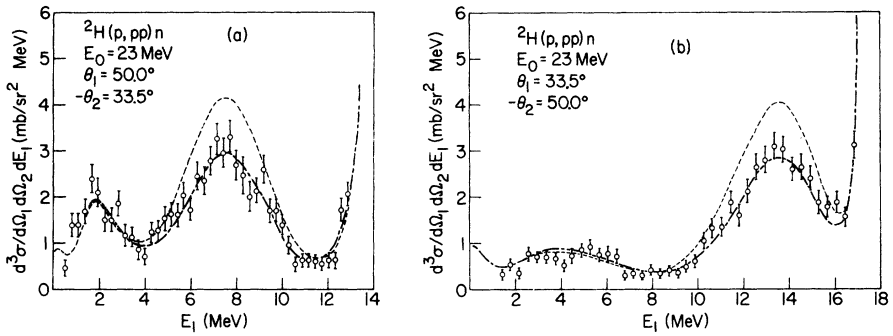

FIG. 5. Observed and calculated spectra: (a) $\theta_1 = 50.0°$, $\theta_2 = -33.5°$; (b) $\theta_1 = 33.5$, $\theta_2 = -50.0°$. The two curves represent potentials A (--) and B (— -).

amplitudes is better than the agreement between the cross sections. This difference is to be expected because (1) linear combinations of three-body amplitudes can cancel, (2) if there is a good deal of cancellation between different partial-wave amplitudes, a small error in each individual partial-wave amplitude can lead to a magnified error in the final summed result, and (3) amplitudes are squared in calculating cross sections. Therefore, the spread in the cross sections at the QFS peak for $\theta_1 = -\theta_2 = 41.7°$ is not unreasonable.

Another source of error may come from the interpolations required to obtain values of the Faddeev amplitudes at momenta for which the integral equation is not explicitly solved. Unless one knows in advance what the kinematic conditions will be and is willing to solve the integral equations for a great many values of q_i, an interpolation or fitting procedure is necessary. Wallace actually solves the integral equation where needed (a time consuming procedure); therefore his calculation is free from fitting errors. Ebenhöh calculates the amplitude at 22 values of the final momentum (q_i) and fits the amplitude to a functional form with 12 parameters. Jain uses three-point Lagrangian interpolation starting from an amplitude calculated at 99 values of q_i. It is likely that Ebenhöh's calculation has more fitting errors than Jain's.

It is difficult to judge which of the three codes is best. Jain's has probably the least numerical inaccuracies, while Wallace's has the most. Ebenhöh's contours seem to have certain numerical advantages. Ebenhöh's results are close to Jain's, while Wallace's results are not precise in certain regions of phase space. Some of the difference in amplitudes is due to slightly different nuclear parameters.[31] The calculations of predictions for various potentials in the next section use the Ebenhöh code; the maximum calculational error of this code is probably only about 2–3% in the cross section—certainly accurate enough for our purposes.

IV. RESULTS AND DISCUSSION

Figures 4–8 present the spectra for the pairs of quasifree angles investigated. The errors shown are statistical, with the absolute error estimated to be less than 3%. This error arises primarily from the interpolation of p-D elastic scattering cross sections. A $d\sigma/d\Omega$ of 58.0 mb/sr was used for the p-D cross section at 30° and 23 MeV. Figure 9 shows the angular distribution of the cross sections at the quasifree peak. The peak cross sections were obtained from semiempirical fits to each spectrum. The fits had a χ^2 per degree of

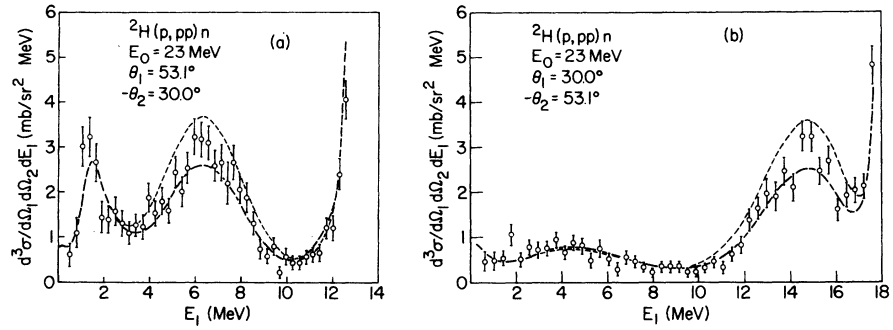

FIG. 6. Observed and calculated spectra: (a) $\theta_1 = 53.1°$, $\theta_2 = -30.0°$; (b) $\theta_1 = 30.0°$, $\theta_2 = -53.1°$. Curves as in Fig. 5.

freedom of approximately 1.0.

Figures 7(a) and 8(a) show the strong final-state interaction peak at low proton energies. Under these conditions, the theoretical results should allow for various experimental effects. Figure 10 shows the effect on the theoretical prediction due to finite angular resolution, finite energy resolution, and energy loss in the target. The angular resolution accounts for only a 0.5% reduction in the height of the FSI peak, as the peak cross section is changing slowly with angle. The finite target thickness has a pronounced effect as very-low-energy protons are being observed. The figures show the total effect calculated for three different target thicknesses.

Figures 4–9 also include the cross section obtained from two separable potential models (A and B) and, in some cases, a third model (C). Also included in Figs. 4, 8(a), and 9 are the single-scattering (i.e., Born) results.

The three potentials employed in our calculations have Yamaguchi form factors, i.e., have momentum-space matrix elements given by

$$\langle \vec{k}| V |\vec{k}'\rangle = -\sum_{n=0}^{1} \lambda_n g_n(k) g_n(k') P_n , \qquad (1)$$

where

$$g_n(k) = N_n(k^2+\beta_n^2)^{-1} .$$

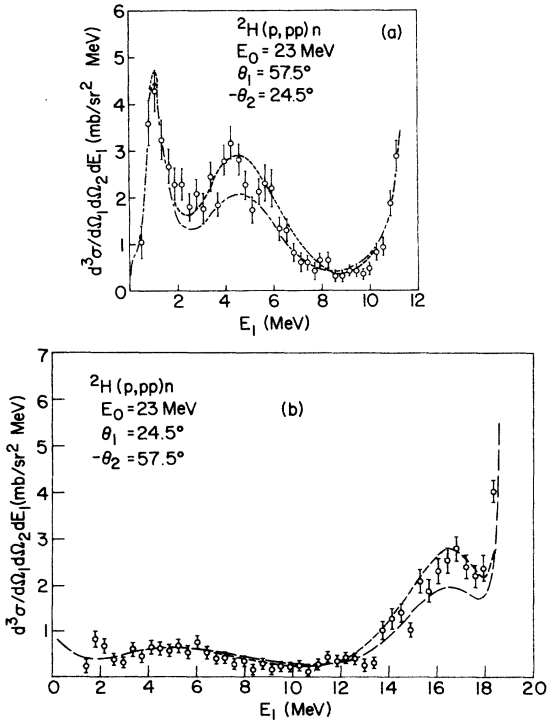

FIG. 7. Observed and calculated spectra: (a) $\theta_1 = 57.5°$, $\theta_2 = -24.5°$; (b) $\theta_1 = 24.5°$, $\theta_2 = -57.5°$. Curves as in Fig. 5.

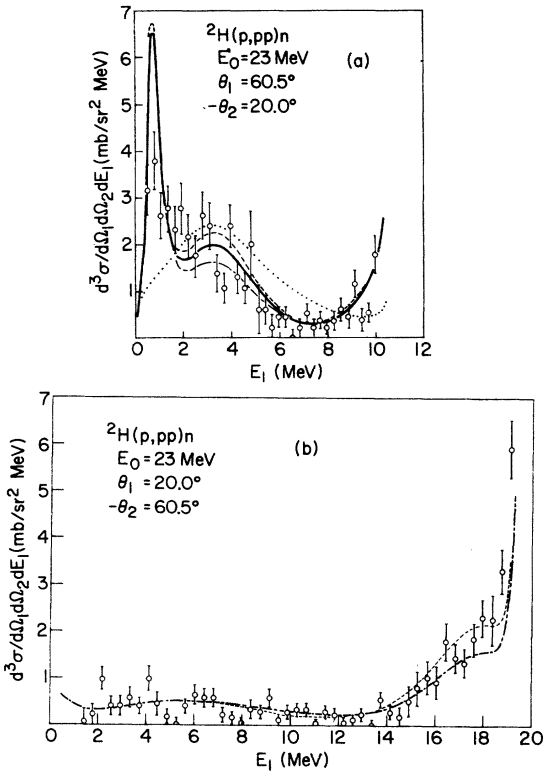

FIG. 8. Observed and calculated spectra: (a) $\theta_1 = 60.5°$, $\theta_2 = -20.0°$, curves as in Fig. 4; (b) $\theta_1 = 20.0°$, $\theta_2 = -60.5°$, curves as in Fig. 5.

The index n indicates the two-body spin-isospin state [$n=0$, spin triplet ($s=1$) isospin singlet; $n=1$, spin singlet ($s=0$) isospin triplet] with projection operator P_n. The numbers N_n, β_n, and λ_n are such

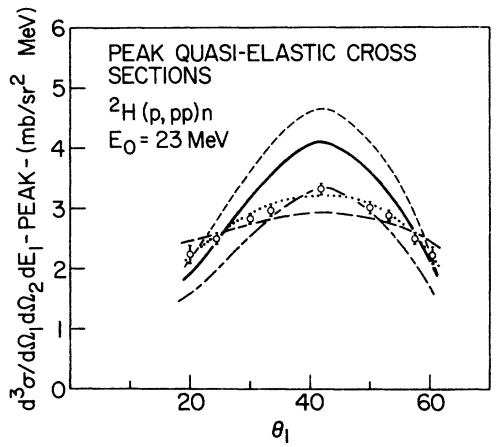

FIG. 9. The cross section at the quasielastic peak plotted as a function of angle. The three curves represent the predictions of the potentials A (--), B (— -), and C (——). The fourth curve (• • •) represents phase space contributions and the fifth (— —) the Born term for potential B ($\times \frac{1}{5}$).

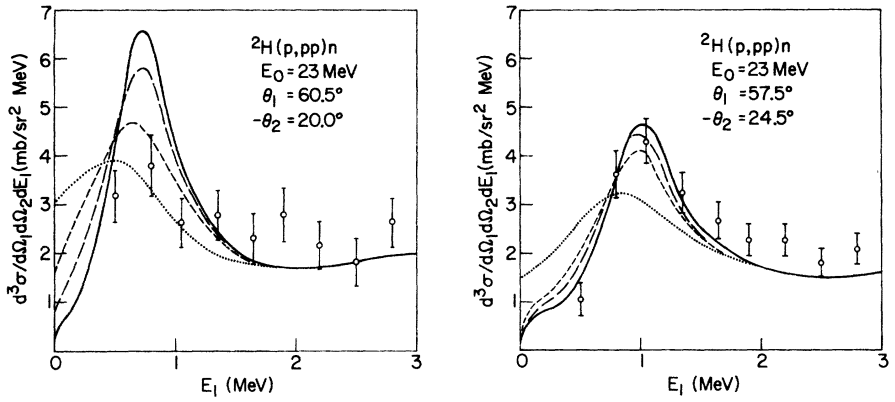

FIG. 10. The theoretical curves of potential *C* for the situation of Figs. 7(a) and 8(a) uncorrected and corrected for target thickness and energy resulution. —— uncorrected, —— 5.0 μm, -- 10 μm, ··· 20 μm. The target used had a nominal thickness of 7.5 μm.

as to give the two-nucleon scattering parameters indicated in Table II (only two of these numbers are independent for each two-body channel). For Yamaguchi form factors the two-nucleon T matrix is given by

$$\langle \vec{k}|\, T(E)\,|\vec{k}'\rangle = \sum_n g_n(k) g_n(k') \tau_n(E) P_n\,, \tag{2}$$

where

$$\tau_n(E) = \frac{(\beta_n - i\sqrt{E})^2}{\kappa_n(\beta_n+\kappa_n)(2\beta_n+\kappa_n - i\sqrt{E})(\kappa_n + i\sqrt{E})}\,.$$

The quantity κ_n satisfies $(\kappa_n+\beta_n)^2(r_{0n}\beta_n - 1) - 2\beta_n{}^2 = 0$ and $\kappa_0{}^2 = E_d$ (deuteron binding energy), and r_{0n} is the effective range.

Potential *A* is the *Y-Y* model of Cahill and Sloan with $a^s_{pp} = a^s_{np} = -23.78$ fm. Potential *B* modifies the *p-p* scattering length to fit the low-energy *p-p* data, $a^s_{pp} = -7.76$ fm. To some degree potential *B* takes into account the Coulomb effect on strong-interaction *p-p* phase shifts. This is the same potential Ebenhöh uses; the *n-p* portion of the potential differs only very slightly from that in potential *A*.

TABLE II. Potential parameters and effective range parameters.

	Potential	
	A	*B*, *C*
a_0 = triplet (fm) [a]	5.423	5.415
r_{00} (fm)	1.76	1.75
E_D (MeV)	2.2246	2.2246
β_0 (fm^{-1})	1.405 81	1.415 47
κ_0 (fm^{-1}) [b]	0.231 61	0.231 61
a_1^{pp} = singlet (fm) [a]	−23.78	−7.76
r_{01}^{pp} (fm)	2.67	2.86
β_1^{pp} (fm^{-1})	1.177 11	1.199 18
κ_1^{pp} (fm^{-1})	−0.039 92	−0.111 19
a_1^{np} (fm) [a]	−23.78	−23.68
r_{01}^{np} (fm)	2.67	2.67
β_1^{np} (fm^{-1})	1.177 11	1.177 33
κ_1^{np} (fm^{-1})	−0.039 92	−0.040 08

[a] As calculated from the effective range formula, $\kappa_i - \frac{1}{2} r_{0i}\kappa_i{}^2 = 1/a_i$.
[b] The κ_i are defined in Ref. 8.

Potential *C* uses the same form factors and parameters as potential *B*, except with the two-body T matrix modified by

$$\langle \vec{k}|\, T(E)\,|\vec{k}'\rangle = \sum_n g_n(k) g_n(k') \tau_n'(E) P_n\,, \tag{3}$$

where

$$\tau_n'(E) = \tau_n(E)\rho_n(E)\{1 - 2\pi^2 i E^{1/2} g_n{}^2(E^{1/2})\tau_n(E) \times [1-\rho_n(E)]\}^{-1} \tag{4}$$

and

$$\rho_n(E) = 1 + [(E+\kappa_n{}^2)/(E_0+\kappa_n{}^2)]\,\Delta_n(1+e^{-\beta E})^{-1}\,.$$

The parameters E_0, Δ_n, and β are chosen such that the on-shell T matrix elements ($E = k^2 = k'^2$) lead to two-nucleon cross sections that give good fits to experiment. For potential *C*, the parameters $E_0 = 15$ MeV, $\beta = \frac{1}{3}$ (MeV)$^{-1}$, $\Delta_1(p\text{-}p) = 0.291$, $\Delta_1(n\text{-}p) = \Delta_0(n\text{-}p) = 0$ yield a good fit to the experimental *p-p* and *n-p* cross sections at 90° (c.m.) and up to 30 MeV (lab). The *p-p* 90° (c.m.) cross sections for each potential and the cross sections obtained from experimental phase shifts[32] appear in Fig. 11. The T-matrix modification of Eqs. (3) and (4) is similar to that employed by Wallace.[19] Equation (4) assures that the two-body K matrix (i.e., principal value T matrix) is multiplied by $\rho_n(E)$ rather than the two-body T matrix as in Wallace's method. Since the K matrix is real

$[\langle k|K(k^2)|k\rangle = -\tan\delta(k)/(2\pi^2 k)$ where $\delta(k)$ is the two-body phase shift] the modifications of Eqs. (3) and (4) retain two-body on-shell and off-shell unitarity. The use of potential C required a minor modification in the basic Ebenhöh computer code.

Two main features manifest themselves in the experimental and theoretical spectra. First is the QFS peak that occurs when the momentum (in the lab frame) of the undetected spectator neutron is a minimum. The QFS peak occurs in the Born term as well as in the final result. The second feature is the narrower FSI peak that occurs when an outgoing proton and neutron (undetected) have a minimum relative momentum (near zero). This peak varies from being practically nonexistent at $\theta_1 = -\theta_2 = 41.7°$ to being very pronounced at $\theta_1 = 60.5°$, $\theta_2 = -20°$.

The basic ingredient that accounts for the QFS peak is the behavior of the deuteron wave function which is peaked around zero relative momentum. One can most easily see this feature in the single-scattering (Born) approximation where the cross section is given by

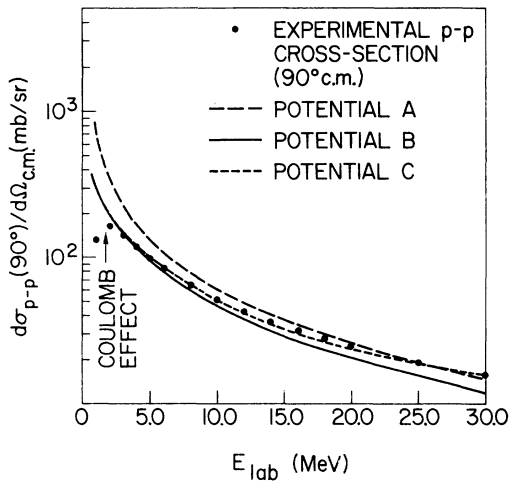

FIG. 11. The free p-p 90° center-of-mass differential cross sections as predicted by potentials A, B, and C and by the phase-shift analysis of the experimental data of Ref. 32.

$$\frac{d^3\sigma}{d\Omega_1 d\Omega_2 dE_1}(\text{Born}) = (\text{kinematic factors})\left[\left(\frac{d\sigma^{pp}}{d\Omega_{c.m.}}\right)^{(3)}_{off}|\phi_0(-\vec{k}_3)|^2 + \left(\frac{d\sigma^{pn}}{d\Omega_{c.m.}}\right)^{(1)}_{off}|\phi_0(-\vec{k}_1)|^2 + \left(\frac{d\sigma^{pn}}{d\Omega_{c.m.}}\right)^{(2)}_{off}|\phi_0(-\vec{k}_2)|^2 + \text{interference terms}\right], \quad (5)$$

where the deuteron wave function $\phi_0(\vec{k}_t)$ is given by

$$\phi_0(\vec{k}_t) = g_0^{np}(k_t)(k_t^2 + \kappa_0^2)^{-1},$$

and $\vec{k}_1$, $\vec{k}_2$, and $\vec{k}_3$ are the momenta of the two protons and the neutron, respectively, in the laboratory system. The half-off-shell cross sections are given by

$$\left(\frac{d\sigma^{pp}}{d\Omega_{c.m.}}\right)^{(3)}_{off} = 4\pi^4|\langle\tfrac{1}{2}(\vec{k}_1-\vec{k}_2)|T_1^{pp}([\tfrac{1}{2}(\vec{k}_1-\vec{k}_2)]^2)|\tfrac{1}{2}(\vec{k}+\vec{k}_3)\rangle|^2,$$

$$\left(\frac{d\sigma^{pn}}{d\Omega_{c.m.}}\right)^{(1)}_{off} = 4\pi^4\{\tfrac{1}{16}|\langle\tfrac{1}{2}(\vec{k}_2-\vec{k}_3)|T_1^{pn}([\tfrac{1}{2}(\vec{k}_2-\vec{k}_3)]^2)|\tfrac{1}{2}(\vec{k}+\vec{k}_1)\rangle|^2 + \tfrac{3}{16}|\langle\tfrac{1}{2}(\vec{k}_2-\vec{k}_3)|T_0^{pn}([\tfrac{1}{2}(\vec{k}_2-\vec{k}_3)]^2)|\tfrac{1}{2}(\vec{k}+\vec{k}_1)\rangle|^2\},$$

$$\left(\frac{d\sigma^{pn}}{d\Omega_{c.m.}}\right)^{(2)}_{off} = 4\pi^4\{\tfrac{1}{16}|\langle\tfrac{1}{2}(\vec{k}_3-\vec{k}_1)|T_1^{pn}([\tfrac{1}{2}(\vec{k}_3-\vec{k}_1)]^2)|\tfrac{1}{2}(\vec{k}+\vec{k}_2)\rangle|^2 + \tfrac{3}{16}|\langle\tfrac{1}{2}(\vec{k}_3-\vec{k}_1)|T_0^{pn}([\tfrac{1}{2}(\vec{k}_3-\vec{k}_1)]^2)|\tfrac{1}{2}(\vec{k}+\vec{k}_2)\rangle|^2\},$$

where T_n indicates the two-body T matrix in spin-isospin channel n [see definitions after Eq. (1)], and $\vec{k}$ is the momentum of the incoming proton in the lab frame. At the QFS peak $\vec{k}_3 \approx 0$; therefore, the term with $|\phi_0(-\vec{k}_3)|^2$ in Eq. (5) dominates. If one approximates the cross section by the first term on the right-hand side of Eq. (5) [this is referred to as the plane-wave-impulse approximation (PWIA)], the only T matrix element that comes into play is

$$\langle\tfrac{1}{2}(\vec{k}_1-\vec{k}_2)|T_1([\tfrac{1}{2}(\vec{k}_1-\vec{k}_2)]^2)|\tfrac{1}{2}(\vec{k}+\vec{k}_3)\rangle.$$

At the QFS peak, this T matrix element is nearly on shell (i.e., $|\vec{k}_1-\vec{k}_2| \approx |\vec{k}+\vec{k}_3|$); consequently, it can be approximated by the on-shell T matrix element[33] which can be directly extracted from the p-p data. The PWIA is not the whole story since the multiple scattering series does not converge at the low energies under consideration. However, the QFS peak does survive in the fully summed scattering series although its magnitude is much smaller and its shape altered [see Figs. 4 and 8(a)].

The FSI peak occurs mainly because the n-p two-body scattering amplitude has a narrow singlet-S

virtual state at zero relative energy. This peak is not seen in single scattering since it is weighted by the momentum tail of the deuteron wave function. At $\theta_1 = 60.5°$, $\theta_2 = -20°$, the FSI contribution to the Born term [Eq. (5)] is weighted by $\phi_0(-\vec{k}_2)$ (here $\vec{k}_3 = \vec{k}_1$) compared with $\phi_0(-\vec{k}_3)$ for the PWIA term. As $E_2 = 19.4$ MeV [$E_2 = (\hbar^2/2m)k_2^2$], and $E_3 = 0.6$ MeV, $\phi_0(-\vec{k}_2)$ is down by a factor of 17 from $\phi_0(-\vec{k}_3)$. The FSI makes itself felt in multiple scattering leading to a strong, narrow peak when the n-p relative energy is close to zero.

According to Migdal-Watson theory, the shape of the FSI peak is given by $d\sigma/(d\Omega_1 d\Omega_2 dE_1) \approx$ (kinematic factors) $(\kappa^2 + p^2)^{-1}$ where $\vec{p}$ is the relative n-p momentum, and $(\kappa - \frac{1}{2}r_0\kappa^2) \approx 1/a$ where a is the scattering length and r_0 is the effective range. One has to be extremely close to $p = 0$ to see this peak because of the large value of the n-p singlet scattering length. At $\theta_1 = -\theta_2 = 41.7°$, the minimum relative energy is 0.25 MeV while at $\theta_1 = 60.5°$, $\theta_2 = -20°$, the minimum relative energy is 0.02 MeV. We observe from Fig. 4 (41.7°, −41.7°) and Fig. 8(a) (60.5°, −20°) how critically the n-p FSI peak depends on this minimum energy. Although not shown in the figures, the Migdal-Watson singlet shape corresponds almost exactly to that predicted by the exact theory.

Multiple-scattering effects also play an important role in understanding the spectra. The full breakup cross section is given by

$$\frac{d^3\sigma}{d\Omega_1 d\Omega_2 dE_1} = (\text{kinematic factors})|T_N|^2, \tag{6}$$

where

$$|T_N|^2 = \tfrac{1}{3}|M_{D1}|^2 + \tfrac{1}{3}|M_{D2}|^2 + \tfrac{2}{3}|M_Q|^2 .$$

The two doublet (M_{D1}, M_{D2}) and quartet (M_Q) matrix elements can be expressed in terms of breakup amplitudes as follows:

$$\begin{aligned} M_{D1} &= -\tfrac{1}{6}\sqrt{3}\,T_{1n\hat{p}}^{1/2}(1) + \tfrac{1}{12}\sqrt{3}\,T_{1n\hat{p}}^{1/2}(2) + \tfrac{1}{4}\sqrt{3}\,T_{0n\hat{p}}^{1/2}(2) \\ &\quad - \tfrac{1}{6}\sqrt{3}\,T_{1\hat{p}\hat{p}}^{1/2}(3) , \\ M_{D2} &= -\tfrac{1}{2}T_{0n\hat{p}}^{1/2}(1) - \tfrac{1}{4}T_{0n\hat{p}}^{1/2}(2) + \tfrac{1}{4}T_{1n\hat{p}}^{1/2}(2) + \tfrac{1}{2}T_{1\hat{p}\hat{p}}^{1/2}(3) , \\ M_Q &= -\tfrac{1}{2}T_{0n\hat{p}}^{3/2}(1) + \tfrac{1}{2}T_{0n\hat{p}}^{3/2}(2) . \end{aligned} \tag{7}$$

For separable potentials the breakup amplitudes $T_n^S(i)$ (S = total three-body spin) are solutions to coupled ($S = \frac{1}{2}$) or uncoupled ($S = \frac{3}{2}$) one-dimensional integral equations. The number in parentheses for each $T_n^S(i)$ refers to a pair of nucleons $j, k \neq i$. In the notation of Cahill and Sloan[10]

$$T_n^S(i) = 2N_{n'(n)}^S(\vec{k}_i, \tfrac{1}{2}(\vec{k}_j - \vec{k}_k); k) \quad (i, j, k \text{ cyclic}) ,$$

where $n'(0) = 1$, $n'(1) = 2$ for n-p, $n'(1) = 3$ for pp. In the notation of Ebenhöh

$$T_n^S(i) = \tfrac{3}{8}\sqrt{3}\,T_i((E + \kappa_0^2)^{1/2}, \sigma : S, s = 1)$$

with

$$\sigma_i : S, s_i, \quad \vec{p}_i = \tfrac{1}{2}(\vec{k}_j - \vec{k}_k) \qquad (i, j, k \text{ cyclic}) ,$$

$$q_i = (2\sqrt{3})^{-1}(\vec{k}_j + \vec{k}_k - 2\vec{k}_i)$$

[see Eq. (17) of Ref. 16], where $s_i = 1$ if $n = 0$, and $s_i = 0$ if $n = 1$. The quantities $\vec{k}_1$ and $\vec{k}_2$ are the momenta of the outgoing protons, $\vec{k}_3$ is that of the outgoing neutron, and $\vec{k}$ that of the incoming proton. The index $i = 1$ or 2 implies the two-nucleon label n-p while $i = 3$ indicates the label p-p. Each $T_n^S(i)$ in Eq. (7) can be written as the sum of a single-scattering contribution and a multiple-scattering contribution, i.e.,

$$T_n^S(i) = T_n^S(i)(\text{Born}) + T_n^S(i)(\text{MS}) .$$

Likewise, each matrix element M can be written as the sum of single-scattering (M^{Born}) and multiple-scattering (M^{MS}) contributions. Therefore, $|T_N|^2$ becomes

$$|T_N|^2 = \tfrac{1}{3}(|M_{D1}^{\text{Born}}|^2 + |M_{D2}^{\text{Born}}|^2 + 2|M_Q^{\text{Born}}|^2) + \tfrac{1}{3}(|M_{D1}^{\text{MS}}|^2 + |M_{D2}^{\text{MS}}|^2 + 2|M_Q^{\text{MS}}|^2) + \text{cross or "interference" terms} . \tag{8}$$

In Figs. 12 and 13 we illustrate the contributions to the cross sections due to single scattering [i.e., the first term in Eq. (8)], multiple scattering (the second term), and interference. Except in the FSI region, the multiple-scattering contribution is relatively flat. The multiple scattering interferes destructively with the Born term. At both $\theta_1 = -\theta_2 = 41.7°$ (Fig. 12) and $\theta_1 = 60.5°$, $\theta_2 = -20°$ (Fig. 13), the resulting QFS peak is much reduced and less pronounced than in single scattering.

Another way to look at QFS, FSI, and interference effects is to investigate various contributions to the fully summed Faddeev amplitudes and the resulting cross section. As in Eq. (8), one can write each M matrix element as the sum of "n-p" terms [contributions of $T_n^S(i) = 1, 2$] and a p-p term [contributions of $T_n^S(3)$], i.e.,

$$M_\alpha = M_\alpha^{n\hat{p}}(i = 1, 2 \text{ contributions}) + M_\alpha^{\hat{p}\hat{p}}(i = 3 \text{ contributions}) .$$

Likewise, $|T_N|^2$ becomes

$$|T_N|^2 = \tfrac{1}{3}(|M_{D1}^{n\hat{p}}|^2 + |M_{D2}^{n\hat{p}}|^2 + 2|M_Q^{n\hat{p}}|^2) + \tfrac{1}{3}(|M_{D1}^{\hat{p}\hat{p}}|^2 + |M_{D2}^{\hat{p}\hat{p}}|^2 + 2|M_Q^{\hat{p}\hat{p}}|^2) + \text{interference terms} . \tag{9}$$

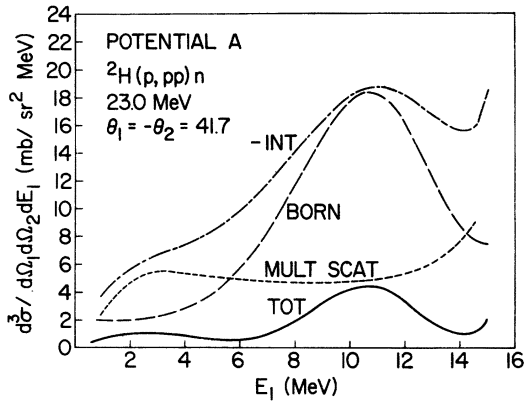

FIG. 12. The Born, multiple scattering, and interference contributions to the $^2H(p,pp)n$ differential cross section at $\theta_1 = -\theta_2 = 41.7°$ for potential A.

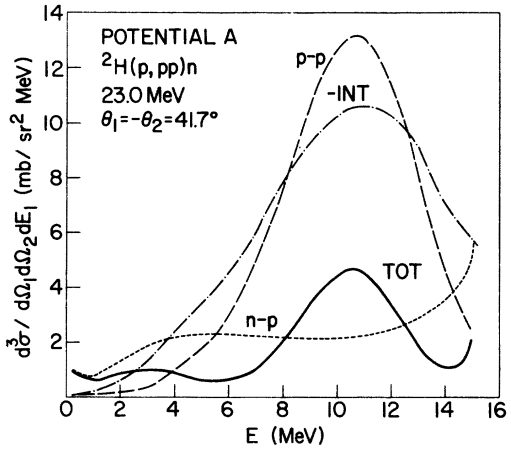

FIG. 14. The p-p, n-p, and interference contributions to the $^2H(p,pp)n$ differential cross section at $\theta_1 = -\theta_2 = 41.7°$ for potential A.

In Figs. 14 and 15, we indicate the contributions to the cross sections for potential A at 41.7°, −41.7° and 60.5°, −20° from Faddeev p-p and n-p amplitudes and interference (INT). Figures 16 and 17 show corresponding curves for potential B. The "n-p" curve corresponds to the first term in Eq. (9), the "p-p" curve corresponds to the second term, and INT corresponds to the sum of all cross terms.

The final cross section results from the destructive interference of a peaked p-p term with a flat n-p term. Of course, the n-p term contributes the FSI peak in the 60.5°, −20° spectrum. The n-p contributions to the FSI peak differ slightly in Fig. 15 (0.742 mb/sr^{2}MeV) and in Fig. 17 (0.718 mb/sr^2 MeV) although the n-p interactions are virtually identical. The difference occurs because the n-p Faddeev amplitudes contain the sum of all multiple scatterings where only the last scattering is restricted to be between a neutron and proton. Multiple scatterings that include p-p interactions do contribute to the n-p amplitude at the FSI peak. One can also understand this difference in terms of Amado's observation that two-body information is distributed in the entire summed Faddeev amplitude rather than in any one contribution.[26] Nevertheless, the shapes of the p-p and n-p contributions have the qualitative features one would expect from p-p and n-p scattering alone (QFS for p-p, FSI for n-p).

One can easily understand the differences in predicted QFS cross sections of potentials A and B in terms of the predicted p-p two-body cross section. The p-p cross sections given by potential A are consistently higher than those predicted by poten-

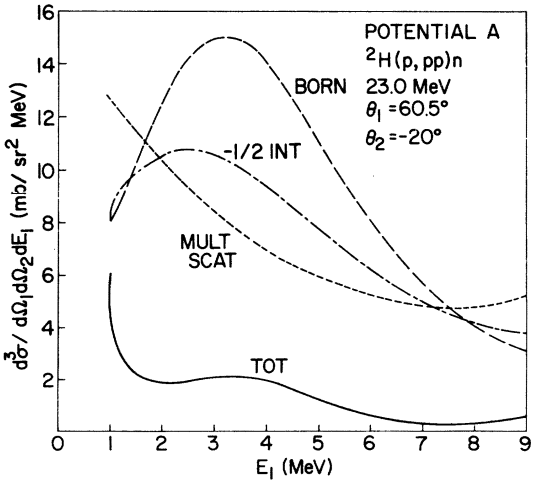

FIG. 13. The Born, multiple-scattering, and interference contributions to the $^2H(p,pp)n$ differential cross section at $\theta_1 = 60.5°$, $\theta_2 = -20°$ for potential A.

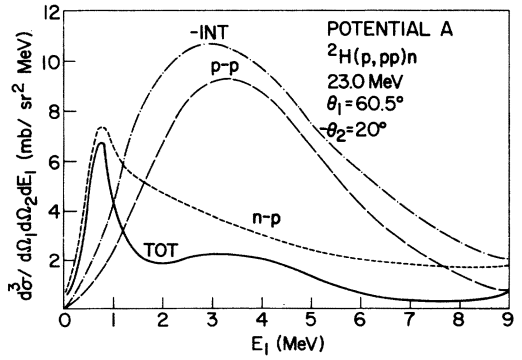

FIG. 15. The p-p, and n-p, and interference contributions to the $^2H(p,pp)n$ differential cross section at $\theta_1 = 60.5°$, $\theta_2 = -20°$ for potential A.

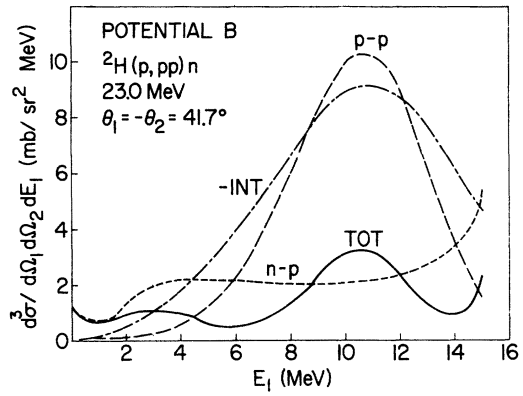

FIG. 16. The *p-p*, *n-p*, and interference contributions to the ^{2}H(*p*,*pp*)*n* differential cross section at $\theta_1 = -\theta_2 = 41.7°$ for potential *B*.

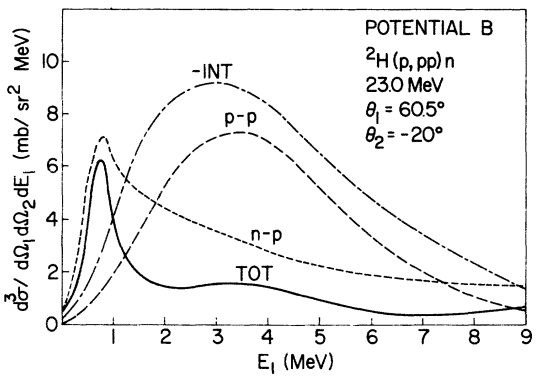

FIG. 17. The *p-p*, *n-p*, and interference contributions to the ^{2}H(*p*,*pp*)*n* differential cross section at $\theta_1 = 60.5°$, $\theta_2 = -20°$ for potential *B*.

tial *B* (see Fig. 11). The 20% difference in the QFS peak cross sections in single scattering (Figs. 4, 8, and 9) is fully consistent with the 20% difference in free *p-p* cross sections (the relevant lab energy is about 18 MeV—see Fig. 11). The final predicted cross sections differ by about 30%; however, the *p-p* Faddeev contributions (Figs. 14 and 16) differ by 20%. Therefore, the difference between potentials at the QFS peak is magnified percentagewise by the strong destructive interference of the *n-p* contributions.

As one approaches the FSI peaks, the differences in predicted cross sections of potentials *A* and *B* become smaller. Here, the almost identical *n-p* interactions dominate the picture. There is a residual (about 7%) difference between potentials at the FSI peak, with potential *A* again predicting the greater cross section. This difference is due to differences in the *p-p* contributions (1.54 mb/sr^2 MeV for potential *A* vs 1.21 mb/sr^{2}MeV) and in the *n-p* contribution (7.42 mb/sr^{2}MeV for potential *A* vs 7.18 mb/sr^{2}MeV) and interference (−2.23 mb/sr^{2}MeV for potential *A* vs −2.15 mb/sr^{2}MeV for *B*). The *p-p* and *n-p* contributions to the difference in heights of the FSI peak underscore the observations that two-body information is distributed in all of the Faddeev amplitudes.

In general, all the potentials studied give good fits to the data. The good agreement is readily apparent in the spectra of Figs. 4–8. The FSI peak observed in Fig. 8(a) is consistent with that predicted by the separable potentials if one folds the experimental effects into the calculation (Fig. 10). There is one notable discrepancy that does occur as can be seen in Fig. 9. The angular distributions of the QFS peaks as calculated from the separable potentials do not agree with experiment; the data are more nearly isotropic than the predictions.

The reason for the discrepancies regarding the angular distribution of the QFS peak cross sections is difficult to pinpoint. At 41.7°, potential *B* is close to experiment, while at 60.5 or 20°, potential *A* does better. Potential *C*, which gives the best fit to the two-nucleon (*N-N*) data, gives a slightly better over-all result than potentials *A* or *B*. The relative energy of the outgoing protons is 9.1 MeV (this would correspond to 18.2 MeV lab). One should remember that multiple scattering effects are important, and in multiple scattering, the relative *p-p* energy can range from 13.1 MeV (26.2 MeV lab) to negative infinity. Potential *C*, one recalls, gives a very good fit to the experimental *N-N* data up to 30 MeV lab (Fig. 11). This potential, therefore, gives a good representation of the *N-N* data relevant to the 23 MeV breakup experiment. It appears that fitting the *N-N* data alone is not sufficient for predicting the correct QFS angular distribution.

If a precise fit to the *N-N* data alone cannot guarantee the proper QFS angular distribution, what other factors may come into play? Recall that the destructive interference of the *n-p* amplitude with the *p-p* amplitude plays an important role in explaining the QFS data. Even slight changes in individual amplitudes could make significant changes in the QFS peaks due to the important destructive interference. Also, the relative strengths of the *p-p*, *n-p*, and interference contributions vary with angle. Therefore, the influence of changes in the *N-N* interaction on the QFS peak could be angle dependent. We have already discovered that changing the energy dependence of the *p-p* *T* matrix without changing the form factor merely accomplishes a renormalization of the QFS angular distribution. The shape calculated

from a Yamaguchi form factor seems always in disagreement with experiment. Thus, it would be worthwhile to investigate the effect of varying the two-nucleon form factors on the angular distributions of Fig. 9. From Eq. (2), changes in the form factor would lead to different types of off-shell variation in two-nucleon T matrix elements. One could retain the same on-shell results by introducing an energy dependence as in Eqs. (3) and (4). Off-shell changes have been studied in the triton problem,[29] but not for deuteron breakup.

If improved fits to the N-N data and improved N-N form factors fail to account for the QFS angular distribution, one must seriously consider the role of the Coulomb interaction. Coulomb effects are important if the two-body p-p angle is small or if the p-p relative energy is close to zero. At 90° p-p angle, for example, Coulomb effects are important for $E_{lab} \leq 3$ MeV (see Fig. 11). In single scattering, the p-p angle and energy are large enough that the Coulomb interaction is unimportant. However, in multiple scattering, the p-p angle takes on all values and the relative energy takes on all values less than 13.1 MeV. It does not appear profitable at this time to investigate the Coulomb effects by comparing p-p and p-n quasifree scattering. The large differences observed in these two mechanisms are associated primarily with interference effects.

The P wave and higher partial waves in the N-N interaction could also play a role in quasifree scattering. The P waves could bring some additional angular dependence since the direction (but not the magnitude) of the relative p-p final-state momentum varies significantly with angle in Fig. 9. The effect of P waves, however, should be small because even at the maximum p-p relative energy (13.1 MeV), P waves play only a very minor role in predicting two-body p-p cross sections.[34] Their importance also decreases with decreasing energy.

One of the main reasons for attempting the three-body problem is to gain information concerning the off-shell N-N interaction and three-body forces.[35] We have suggested that the influence of off-shell effects on the QFS angular distribution should be studied by varying N-N form factors. Different N-N form factors most likely also play a role in predicting the FSI peak. In particular, the FSI peak should be primarily sensitive to the zero-energy N-N interaction, both on shell and off shell. The triton binding energy, also, is primarily sensitive to the zero-energy off-shell N-N T matrix.[29] The FSI peak in deuteron breakup is primarily the result of a two-body process. In the triton, three-body forces may play a different role than at the final-state peak for the $^2H(p, pp)n$ reaction since the three nucleons are on the average closer together than in the scattering process. Therefore, any gross incompatability in the zero-energy T matrix as "measured" by the triton binding energy and by deuteron breakup could be indicative of the presence of three-body forces. The presence of such forces has been indicated by both meson-theoretic and phenomenological considerations.

At present, it is extremely difficult to disentangle the roles of the many different effects (Coulomb, P-wave, off-shell, and three-body forces) that could contribute to breakup cross sections. One should start searching for regions of sensitivity to various effects. The easiest effect to study, and the first one that should be studied is that of off-shell effects by varying the N-N form factors.

V. CONCLUSIONS

Calculations of the cross sections for the $^2H(p, pp)n$ reaction based on the Amado model are in good agreement with our experimental measurements. The agreement is better in some portions of phase space than in others, depending upon the potential used, indicating that the calculations work well but not perfectly. The computer codes that exist for the solutions can no longer be used blindly. They describe the basic features of the interaction, but the details of agreement of experiment and calculations depend upon the details of the potentials used.

Data was compared with the predictions of three potentials. These potentials differed primarily in the strength of the proton-proton interaction. Discrepancies as large as 30% exist between theory and experiment with regards to the height of the QFS peaks. Moreover, for all of the potentials considered, the shape of the calculated angular distribution of QFS peaks is not in close agreement with experiment. Three computer codes were also compared, and, in their regions of validity their results differ by at most a few percent.

The calculations indicate that interference is very important. At the QFS peak the p-p amplitudes, the n-p amplitude, and interference all play important roles. Consequently, changes in either the p-p or n-p interaction could have important consequences in improving the agreement with experiment. We feel that it is necessary but not sufficient to use p-p interactions that give good fits to the two-body cross sections over a fairly large range of energies. As mentioned in Sec. IV, both the height of the FSI peak and triton binding are likely very sensitive to the off-shell variation in the zero-energy two-nucleon T matrix. One can study the influences of this off-shell variation by varying the two-nucleon form factors in three-

body breakup or bound-state calculations. Experimentally, one should consider measuring the FSI peaks over a range of projectile energies [this suggestion holds for (p,pp), (p,pn), (n,nn), and (p,np) reactions]. An interesting problem would then be to investigate whether form factors that give a correct description of the experimental FSI peaks give the correct triton binding energy. The results of such an investigation could have a bearing on the role of three-body forces. For such a study to be conclusive, one should search for form factors that fit the experimental FSI peaks over a range of projectile energies. One can thus be assured that one is sampling T matrix elements roughly equivalent to those relevant for the triton problem (see Ref. 29). As has been pointed out in this paper, one must be extremely careful in obtaining the final-state cross sections and in comparing experiment with theory in this region.

It appears that improved fits to the p-p data alone will not explain the QFS angular distribution. Since the p-p and n-p interaction and interference effects all have an important bearing on the predicted QFS peaks, variations in the N-N form factor could affect the calculations of the QFS peaks. It is important that efforts to improve agreement with the QFS angular distribution should continue to describe the FSI peaks. The result of such investigations may indicate how much physics we can obtain from a simple S-wave separable-potential model. We would also hope to get some idea of the extent to which we could ignore Coulomb and P-wave effects. The results of this paper call for calculations with, hopefully, improved two-nucleon form factors. The success or failure of such future calculations will indicate to what extent we can ignore the more sophisticated aspects of the internucleon force.

ACKNOWLEDGMENTS

The authors are grateful for the support of the cyclotron operations staff under the direction of George E. Miller. We would like to thank W. Ebenhöh, W. Breunlich, and I. Šlaus for communications and discussion and J. McElhinney for his continued interest.

---

*Present address: Los Alamos Scientific Laboratory, Los Alamos, New Mexico 87544.

[1]L. D. Faddeev, Zh. Eksp. Teor. Fiz. 39, 1459 (1960) [transl.: Sov. Phys.—JETP 12, 1014 (1961)].
[2]A. N. Mitra, Nucl. Phys. 32, 529 (1962).
[3]R. Aaron, R. D. Amado, and Y. Y. Yam, Phys. Rev. 140, B1291 (1965).
[4]R. Aaron and R. D. Amado, Phys. Rev. 150, 857 (1966).
[5]C. Lovelace, Phys. Rev. 135, B1225 (1964).
[6]A. C. Phillips, Phys. Rev. 142, 984 (1966).
[7]W. M. Kloet and J. A. Tjon, Phys. Lett. 37B, 460 (1971).
[8]R. T. Cahill and I. H. Sloan, Phys. Lett. 33B, 195 (1970).
[9]S. Oryu, Prog. Theor. Phys. 44, 1208 (1970).
[10]R. T. Cahill and I. H. Sloan, Nucl. Phys. A165, 161 (1971).
[11]R. T. Cahill, Nucl. Phys. A185, 236 (1972).
[12]D. J. Margaziotis, J. C. Young, I. Šlaus, G. Anzelon, F. P. Brady, and R. T. Cahill, Phys. Lett. 37B, 263 (1971).
[13]I. Šlaus, J. W. Sunier, G. Thompson, J. C. Young, J. W. Verba, D. J. Margaziotis, P. Doherty, and R. T. Cahill, Phys. Rev. Lett. 26, 789 (1971).
[14]R. Bouchez, S. Desreumaux, J. C. Gondrand, C. Perrin, P. Perrin, and R. T. Cahill, Nucl. Phys. A185, 166 (1972).
[15]J. Sanada, S. Seki, and S. Oryu, Phys. Lett. 40B, 546 (1972).
[16]W. Ebenhöh, Nucl. Phys. A191, 97 (1972).
[17]B. Zeitnitz, R. Maschuw, P. Suhr, and W. Ebenhöh, Phys. Rev. Lett. 28, 1656 (1972).
[18]H. Klein, H. Eichner, H. J. Helten, H. Kretzer, K. Prescher, H. Stehle, and W. W. Wohlfarth, Nucl. Phys. A199, 169 (1973).
[19]J. M. Wallace, Phys. Rev. C 7, 10 (1973).
[20]E. L. Petersen, R. G. Allas, R. O. Bondelid, A. G. Pieper, and R. B. Theus, Phys. Lett. 31B, 209 (1970).
[21]E. L. Petersen, R. G. Allas, R. O. Bondelid, D. I. Bonbright, A. G. Pieper, and R. B. Theus, Phys. Rev. Lett. 27, 1454 (1971).
[22]D. J. Margaziotis, G. Paic, J. C. Young, J. W. Verba, W. J. Braithwaite, J. M. Cameron, D. W. Storm, and T. A. Cahill, Phys. Rev. C 2, 2050 (1970).
[23]J. L. Durand, J. Arvieux, A. Fiore, and C. Perrin, Phys. Rev. C 4, 1957 (1971).
[24]M. Jain and C. Doolen, Bull. Am. Phys. Soc. 18, 125 (1973).
[25]Y. Yamaguchi, Phys. Rev. 95, 1628 (1954).
[26]R. D. Amado, Phys. Rev. 158, 1414 (1967).
[27]R. D. Amado and J. V. Noble, Phys. Rev. 185, 1993 (1969).
[28]J. G. Rogers, D. P. Saylor, J. D. Bronson, and M. Jain, Phys. Rev. Lett. 17, 1181 (1972).
[29]M. I. Haftel, Phys. Rev. C 7, 80 (1973).
[30]Energies here are expressed in units of momentum squared, i.e., $E(\text{fm}^{-2}) = (M/\hbar^2)E(\text{MeV})$.
[31]For example, the three codes use different nuclear masses; Jain uses $M = 939.20$ MeV, Wallace uses $M = 938.92$ MeV, and Ebenhöh uses $M = 938.86$ MeV. Also, Jain and Wallace determine β,λ by fitting the triplet scattering length and deuteron binding energy; Ebenhöh fits the deuteron binding energy and effective range. For example, β_1(Wallace) = 1.407 fm^{-1}, β_1(Ebenhöh) = 1.406 fm^{-1}, κ_1(Wallace) = 0.231 fm^{-1}, κ_1(Ebenhöh) = 0.2316 fm^{-1}. The Wallace code seems slightly more sensitive to very small changes in potential parameters than does the Ebenhöh code.
[32]M. H. MacGregor, R. A. Arndt, and R. M. Wright, Phys. Rev. 169, 1128 (1968); 173, 1272 (1968); 182,

1714 (1969).
[33]I. E. McCarthy and P. C. Tandy, Nucl. Phys. A178, 1 (1971).
[34]P waves contribute very little to p-p scattering, and probably little to p-pp scattering because of the spin-orbit splitting in the triplet P states. They do play a major role, however, in polarization experiments.
[35]Various authors, in *Proceedings of the International Conference on Few Particle Problems in the Nuclear Interaction, Los Angeles, 1972,* edited by I. Šlaus, S. A. Moskowski, R. P. Haddock, and W. T. H. van Oers (North-Holland, Amsterdam, 1972).